AAS 23-306

JETTISON AND DISPOSAL FROM NEAR RECTILINEAR HALO ORBITS, PART 2: APPLICATIONS

Diane C. Davis,[*] Stephen T. Scheuerle,[†] Steven L. McCarty,[‡] Emily M. Zimovan-Spreen,[§] Brian P. McCarthy,[**] Melissa L. McGuire,[††] and Kathleen C. Howell[‡‡]

Objects deployed from a Near Rectilinear Halo Orbit (NRHO) experience simultaneous gravitational forces from the Moon, the Earth, and the Sun, and post-deployment behavior is complex. The current investigation applies the theories explored in Part 1 of the study to examine the dynamics of objects deployed from the Gateway NRHO to heliocentric space. Examples include jettison of cubesats and logistics modules as well as end-of-life options for the Gateway itself. Recontact risk with the Gateway as each object departs the lunar vicinity is explored, and both the immediate destination and the long-term fate of the deployed objects are assessed.

INTRODUCTION

The Gateway[1] is proposed as an outpost in deep space: a proving ground for deep space technologies and a staging location for missions to the lunar surface and beyond Earth orbit. During its 15-year lifetime, Gateway will host crewed and uncrewed visiting vehicles and serve as a base for various utilization opportunities, which may include cubesat deployments. Cubesats represent deliberate jettisons at low relative velocity up to a few meters per second and may or may not have the capability to do additional maneuvers after the initial jettison. Larger visiting vehicles will also depart the Gateway, including crew vehicles, logistics modules (LMs) filled with waste material or science payloads, and disposable lunar lander modules, which must be safely jettisoned at higher values of relative velocity and may be equipped to perform additional post-jettison maneuvers. Each of these types of objects are subject to complex cislunar dynamics; each must depart the lunar vicinity without recontacting the Gateway and reach its desired destination. This study focuses on jettison to heliocentric orbit.

The current baseline orbit for the Gateway is a 9:2 Near Rectilinear Halo Orbit (NRHO) near the Moon.[2] This NRHO exhibits nearly stable behavior, but over time, any unmaintained object in this orbit departs due to the small instabilities associated with the NRHO. A jettison maneuver speeds the departure from the NRHO, and the effects of the maneuver on the spacecraft behavior depend on the location, magnitude, and direction of the burn. Previous investigations[3,4,5,6] examined departure from the NRHO, including recontact risk and escape from the Earth-Moon vicinity. Part 1 of the current investigation[7] performs a literature review of the jettison topic and then combines components of earlier studies with new analysis to provide a more complete understanding of the design space for objects jettisoned from the NRHO vicinity with the goal of

[*] Gateway Mission Design Lead, Johnson Space Center, Houston TX, diane.c.davis@nasa.gov.
[†] Ph.D. Candidate, School of Aeronautics and Astronautics, Purdue University, sscheuer@purdue.edu.
[‡] PPE Mission Design Engineer, Glenn Research Center, Cleveland OH, steven.mccarty@nasa.gov.
[§] Gateway Mission Design Engineer, Johnson Space Center, Houston TX, emily.m.spreen@nasa.gov.
[**] Gateway Mission Design Engineer, a.i. solutions, Inc., brian.p.mccarthy@nasa.gov.
[††] PPE Mission Design Lead, Glenn Research Center, Cleveland OH, melissa.l.mcguire@nasa.gov.
[‡‡] Hsu Lo Distinguished Professor, School of Aeronautics and Astronautics, Purdue University, howell@purdue.edu.

reaching heliocentric orbit. This paper, part 2 of the current investigation, applies the new cohesive understanding from part 1 to several example problems of deployment from the Gateway NRHO. Post-jettison behavior is examined to ensure the departing object does not threaten to collide with Gateway as it exits the lunar vicinity. Assuming successful departure from the NRHO, the long-term destination of objects jettisoned from the Gateway is explored. Safe disposal options for LMs, lander modules, or debris objects, and science missions for cubesats or other spacecraft, could include deployment to heliocentric space. This investigation demonstrates methods to target NRHO departure conditions that lead to reliable heliocentric escape. Finally, the long-term behavior of spacecraft deployed to heliocentric space is investigated. While general disposal trajectories often result in orbits that achieve heliocentric escape but subsequently return to the Earth-Moon vicinity after many years, specific post-escape conditions can ensure that the jettisoned spacecraft remains far from the Earth-Moon system over long-term propagations. Cleanup maneuvers to ensure escape from the Earth-Moon system in the presence of realistic state and maneuver dispersions are investigated. Finally, the Gateway end-of-life trajectory is assessed. Several options exist for safe disposal of the Gateway itself after decommissioning at the end of its operational life. One potential destination is a long-term heliocentric orbit that avoids encounters with the Earth-Moon system. A low-thrust transfer to heliocentric orbit is discussed, along with optimization methods to ensure a return to the Earth-Moon vicinity is avoided for extended periods of time.

BACKGROUND AND DYNAMICAL MODELS

After a low-thrust spiral transfer from the Earth to the lunar vicinity,[8] the Gateway will reside in a southern L2 NRHO that exhibits a 9:2 resonance with the lunar synodic period. Thus, perilune passage occurs on average every 6.56 days. The baseline NRHO is nearly stable, so that objects jettisoned with a small Δv depart relatively slowly from the lunar vicinity. Phased to avoid long eclipses from the Earth's shadow, the selected resonance results in a repeating pattern of Sun-Earth-Moon-Spacecraft geometry so that the orbit is quasi-periodic in both the Earth-Moon and the Sun-Earth frames. Long-term baseline NRHOs exist in various dynamical models; a concurrent investigation explores the generation of these baseline trajectories.[9] The 15-year NRHO employed in the current analysis[10] is pictured in Earth-Moon and Sun-Earth frames in Figure 1. Note that the simple, quasi-periodic orbit as viewed in the Earth-Moon frame has a repeating pattern with 9 peaks when viewed in the Sun-Earth frame. This 9-revolution pattern is a function of the 9:2 resonance of the NRHO with the lunar synodic period. Note also that the periodicity of the orbit is not exact, and the geometries vary from one revolution to the next when computed in a high-fidelity ephemeris force model. However, the patterns remain significant, and if an object is jettisoned at a given location along the NRHO when viewed in the Earth-Moon rotating frame, that object experiences one of 9 possible orientations with respect to the Sun and Earth. The orientation of the jettison is defined here in terms of a Moon angle, approximating the position of the Moon or the object relative to the Sun-Earth rotating $+X$-axis. A schematic appears in Figure 2. The locations of a jettison at osculating true anomaly TA = 200º during 9 consecutive revolutions are marked; for example, a jettison from TA = 200º during revolution 2 is characterized by a Moon angle of -33º, while a jettison at the same TA during the subsequent revolution has a Moon angle of 47º. The Moon angle shifts by approximately 80º from one revolution to the next. Note that revolution 1 along the baseline NRHO is defined starting from a perilune passage on Jan 8, 2020.

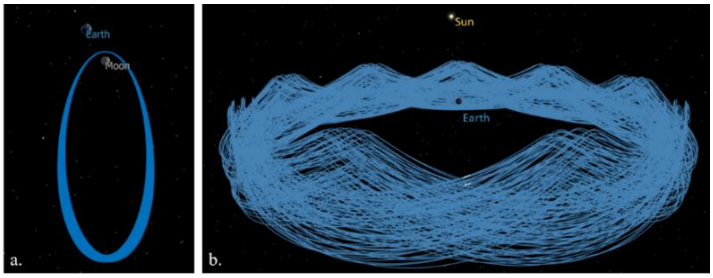

Figure 1. 15-year reference NRHO in Earth-Moon (a) and Sun-Earth (b) rotating views

The examples detailed in this paper are computed using N-body differential equations in the FreeFlyer astrodynamics software package and in the Copernicus optimization software package. Within this analysis, the relative position of each perturbing body with respect to the central body is instantaneously computed by employing NAIF SPICE ephemeris data. The Earth, Sun, and planets are included as point masses, and the

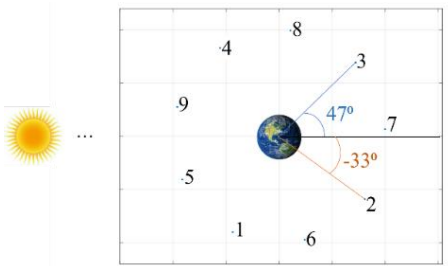

Figure 2. Moon angle definition and jettison locations for jettison at TA = 200° during 9 consecutive NRHO revolutions.

Moon's gravity is modeled using the GRAIL (GRGM660PRIM) model truncated to degree and order 8 unless otherwise specified. Solar radiation pressure (SRP) acting on a sphere is also included in the force model. Maps generated using Circular Restricted 3-Body Problem (CR3BP) and Bicircular Restricted 4-Body Problem (BCR4BP) dynamics are also employed in this analysis. The force models used in the construction of these maps are outlined in part 1 of this investigation.[7] In these models, the Earth-Moon barycenter is denoted B_1, such that the Sun-B_1 model refers to the Sun – Earth-Moon barycenter model.

Locations along the NRHO are referenced in this study in terms of osculating true anomaly (TA), though it is worth noting that in some applications, it is more convenient to use the mean or eccentric anomalies to denote locations along the NRHO. Maneuver directions are parameterized in terms of yaw and pitch relative to the inertial velocity-normal-binormal (VNB) frame. The VNB directions are defined along the orbit such that the V direction aligns with the inertial velocity, $V = (\dot{X}, \dot{Y}, \dot{Z})$, the N direction corresponds to the orbit normal, $N = (X, Y, Z) \times (\dot{X}, \dot{Y}, \dot{Z})$, and B completes the right-handed system. The yaw angle ranges from -180° to 180° in the V-B plane, and the pitch angle ranges from -90° to 90° out of the V-N plane.

Note that for clarity in this investigation, the term "departure" is used to refer to departures from the NRHO or the lunar vicinity. The term "escape" is used to refer to escapes from the Earth-Moon system to heliocentric space. The term "Earthbound" is employed to denote trajectories that are bound to the Earth-Moon system, or those that don't achieve heliocentric escape within the duration of a given propagation.

GOALS FOR SAFE JETTISON IN THE NRHO

Achieving safe jettison or disposal from the Gateway NRHO is a multi-dimensional problem. This investigation focuses on the jettison of objects to heliocentric space, dividing the problem into three regimes, each with its own challenges. The three phases of the jettison problem identified here are 1) safe departure from the lunar vicinity without conjunction risk, 2) successful escape to heliocentric space, and 3) long-term evasion of the Earth-Moon vicinity.

Regime 1: Safe NRHO Departure

The first regime begins immediately after jettison and ends with departure from the lunar vicinity. As previously noted,[5,11] the duration of this first portion of the jettison problem, that is, the time to depart the lunar vicinity, varies as a function of Δv magnitude, direction, and location around the NRHO. For the jettison Δv magnitudes explored here, roughly 1-20 m/s, the time to depart the NRHO varies significantly, from as little as 4 days to as much as 150 days. The fastest departures are observed to occur for jettisons executed near perilune; however, poor state knowledge, challenging attitude dynamics, and high sensitivity to errors in the vicinity of NRHO perilune passage recommend that jettison be avoided within ±120° of perilune in TA, or about ±3.5 hours of perilune passage. A further discussion of the time to depart the NRHO as a function of jettison Δv magnitude, direction, and location, as well as a recommendation to avoid jettison near perilune, appears in Davis et al.[6] In the current work, departure from the NRHO is defined when the departing object exceeds 450,000 km from the Earth, ensuring the object departs through the Earth-Moon L2 portal. Once this radius is exceeded, the object is assumed to have departed the lunar vicinity. On its journey from the Gateway to lunar vicinity exit, the object must avoid hitting the Gateway. In the current study, an object is considered a recontact risk if, after initial departure from a 100 km keep-out sphere around a propagated and maintained Gateway, the object re-enters the keep-out sphere with decreasing range. A safe departure is achieved when the object departs the NRHO without returning within this recontact sphere. Any safe departure must be validated for the specific epoch of the jettison and in the presence of realistic operational errors; thus, robust solutions for safe NRHO departure are sought. To achieve robustness in the solution, two additional factors are prioritized when selecting a safe departure trajectory. First, fast departures are preferred. Each additional revolution around the Moon compounds the effects of modeling and execution errors on the jettison trajectory that can lead to recontact risk in the presence of realistic operational errors. Second, increasing rates of separation at each perilune passage are prioritized. Typically, the range between the jettisoned object and the Gateway reaches a local maximum at each perilune passage. However, as identified

previously,[6] some jettison trajectories experience a flip in this pattern, with a close approach at a perilune passage several revolutions after initial jettison. In the presence of errors, these flips in the range at perilune can lead to unpredictable behavior. Because the range flips at perilune can occur many revolutions downstream from the jettison, and jettison errors are magnified with increasing time, a larger radius of concern is selected. Thus, flips in the range at perilune that result in a close approach under 1000 km are avoided when possible. In summary, the focus in regime 1 is on achieving three goals: selecting jettison conditions that avoid the 100 km keep-out sphere until the object departs the lunar vicinity, achieving fast departure to minimize the buildup of errors, and ensuring increasing Gateway-object range at each perilune passage. Examples of a favorable departure and two unfavorable departures appear in Figure 3. Each is deployed with a jettison Δv of 1.7 m/s from a true anomaly TA = 200º. The trajectories are plotted in the Earth-Moon rotating frame in Figure 3a; they appear similar in behavior as they depart the NRHO. Each departs after approximately 45 days in the lunar vicinity. The range of the jettisoned object relative to the Gateway appears as a function of time past jettison in Figure 3b. The favorable departure case appears in green. After initial jettison, the range increases without returning within the 100 km keep-out sphere or experiencing a perilune range flip below 1000 km. In red, a jettison resulting in a return within the 100 km sphere at the perilune passage following jettison is plotted. Similarly, a jettison that experiences a flip in the range at perilune about two weeks after jettison appears in magenta. The first goal of jettison is to achieve departure trajectories that demonstrate the behavior plotted in green in Figure 3.

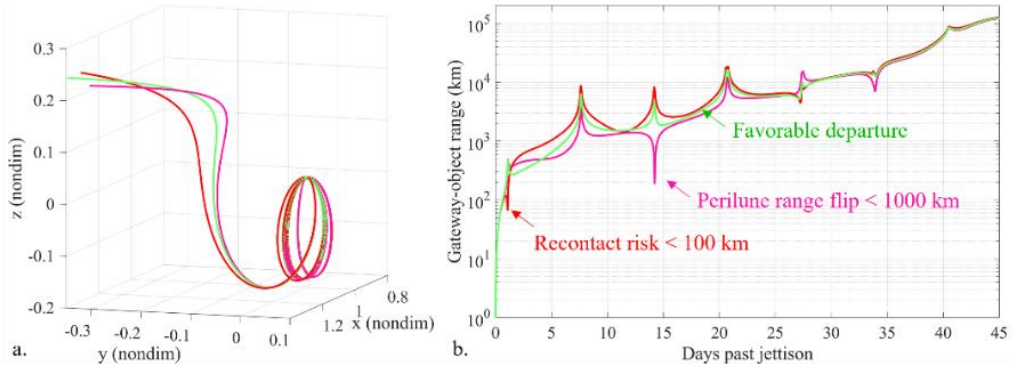

Figure 3. Three departing trajectories after a 1.7 m/s jettison at TA = 200º. Earth-Moon rotating view (a) and Gateway-object range (b).

Regime 2: Escape to heliocentric space

The second goal of jettison in this investigation is to achieve direct escape to heliocentric space. Direct escape is defined here as achieving a distance from the Earth of 1.48 million km, equivalent to 1.5 times the distance to the Sun-Earth libration points, without additional revolutions around the Earth. To escape from the Earth-Moon vicinity, two conditions must be met. First, at departure from the lunar vicinity, the object must possess sufficient energy to escape the Earth's gravitational pull. In terms of CR3BP dynamics, the energy of the trajectory must be sufficient such that the Sun-B_1 zero velocity curves (ZVCs) are open at the libration points.[5] In this investigation, the Sun-B_1 Hamiltonian is employed to compare energetic departures with low-energy departures. In part 1 of this investigation,[7] conditions at NRHO departure are defined to ensure an energetic departure is achieved. In broad terms, the angular momentum of the departing trajectory must be oriented such that lunar gravity increases spacecraft energy; that is, the NRHO departure must mimic an energy-increasing lunar flyby, rather than an energy-decreasing lunar flyby. This condition is achieved when, as written in Earth-Moon rotating coordinates, the following condition is met at departure from the lunar vicinity:

$$x\dot{y} - y\dot{x} \geq 0 \tag{1}$$

Then, once an energetic departure is achieved, the orientation of the departure in the Sun-B_1 frame must be aligned such that solar gravity pulls the trajectory out of the Earth-Moon vicinity. The orientation at departure depends on epoch of the jettison as well as the time to depart the NRHO. For some epochs, or equivalently, for some Sun-B_1 orientations at jettison, the fastest departure from the NRHO yields an unfavorable orientation at NRHO departure, and direct heliocentric escape is not achieved. In these scenarios, a slower departure from the NRHO is required to enable favorable geometry and hence direct escape. Four example

cases appear in Figure 4, each jettisoned with a 1.7 m/s maneuver at TA = 200º. The first three trajectories, in shades of green and blue, all depart the NRHO with sufficient energy to escape the Earth-Moon system. Trajectory 1, in light green, and trajectory 3, in blue, depart the NRHO with a distinctive "corner-turn" geometry previously identified as leading to energetic departures.[5] A second departure geometry, here denoted a "lower departure", is also observed to depart the NRHO with sufficient energy to escape to heliocentric space; trajectory 2, in dark green, is an example of a lower departure. While all three of these energetic departures escape to heliocentric space, only trajectory 1 is an example of a desired escape case. It is observed that, in the presence of errors, lower departures similar to trajectory 2 do not maintain their departure geometry to enable robust escapes to heliocentric space. Trajectory 3 departs with the more favorable corner-turn geometry but with a poor Sun-B_1 orientation. Solar gravity decreases the post-jettison perigee (with, essentially, a backwards ballistic lunar transfer geometry) as observed in Figure 4c in the Sun-B_1 rotating frame. After the additional perigee passage, the object escapes indirectly to heliocentric space through the Sun-B_1 L1 portal. In the presence of errors, this indirect escape to heliocentric space does not prove to be robust; it can lead to Earth impact or additional revolutions around the Earth prior to escape. Trajectory 1 departs with a corner-turn geometry with an orientation that yields direct escape to heliocentric space through the Sun-B_1 L2 portal. Such favorable escapes are observed through both the L1 and L2 portals, depending on the post-departure orientation. It is interesting to note that trajectory 3 departs the NRHO approximately 45 days after jettison, but at that departure epoch, an unfavorable Sun-B_1 orientation prevents direct escape. Trajectories 1 and 2 each depart one revolution later, about 52 days after jettison. At this later departure epoch, the favorable Sun-B_1 geometry allows direct escape. Finally, trajectory 4, plotted in black, departs the NRHO with an unfavorable geometry that does not satisfy Equation 1. With insufficient energy to escape the Earth's gravity, it remains Earthbound longterm.

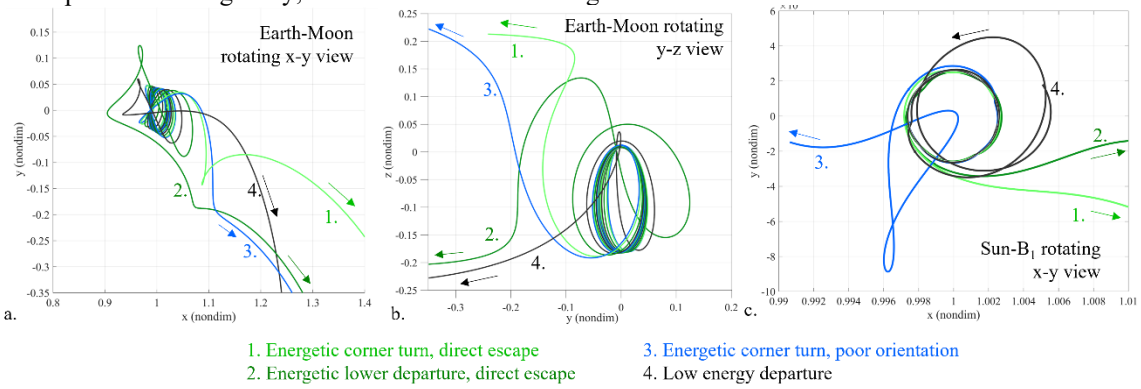

Figure 4. Four departing trajectories after a 1.7 m/s jettison at TA = 200º. Earth-Moon *x-y* (a) and *y-z* (b) rotating views, Sun-B_1 *x-y* rotating view (c).

Thus, to design a jettison that successfully departs the NRHO and escapes to heliocentric space as defined in this investigation, the jettison maneuver must:

- Avoid returning to within 100 km of the Gateway
- Avoid flips in range at perilune that approach within 1000 km of the Gateway
- Depart the NRHO relatively quickly
- Depart with an Earth-Moon geometry that satisfies Equation 1, preferably a corner-turn geometry
- Depart with a Sun-B_1 orientation that allows direct escape

This list of requirements or recommendations for the jettison maneuver significantly restricts the available maneuver directions for a given jettison Δv magnitude, which may be limited by the deployer device or spacecraft capability, and a given jettison TA, which may be limited by operational considerations. A set of jettison maps facilitates the selection of jettison conditions that yield the desired trajectory behavior. The generation of the maps is discussed in part 1 of this investigation;[7] the maps represent an augmentation of the recontact maps introduced previously.[4,11] The maps vary as the jettison Δv magnitude, direction, TA, and Moon angle vary. Two sample maps appear in Figure 5. These maps represent jettison from TA = 200º with Δv = 1.7 m/s during two subsequent revolutions. These two jettison locations are characterized by Moon angles of -33º and 47º, as defined in Figure 2. Each point on the maps represents a maneuver direction, with the yaw and pitch of the maneuver denoted along the horizontal and vertical axes, respectively. Each

maneuver direction is colored according to one of the recommendations for safe jettison. Red points denote jettison directions that result in recontact risk, or returns within the 100 km keep-out sphere. Magenta points represent jettison directions that yield flips in the range at perilune under 1000 km. Jettison directions that yield corner-turn departures are marked in blue. A green background denotes maneuvers that directly escape to heliocentric space, while a black background represents jettison directions that do not yield direct heliocentric escape. Thus, a maneuver direction that yields immediate recontact risk, then experiences a flip in perilune range and fails to directly escape to heliocentric space is represented by the overlap of red, pink, and black directions. Such a maneuver would not be advised. A direction that is colored blue over a black background yields an energetic corner-turn departure with poor orientation, as in trajectory 3 in Figure 4. A yaw/pitch combination that results in a lower departure that directly escapes to heliocentric orbit is colored green, without blue overlaid. An example is trajectory 2 in Figure 4. The desired combination is blue overlaid on a green background, far from red or pink points. Such a combination results in an energetic corner-turn departure that directly escapes to heliocentric space without risk of recontact with the Gateway. The selected maneuver directions that yield the trajectories depicted in Figure 3 are marked on the map with circles in Figure 5b, and the jettisons from Figure 4 are denoted by circles and numbers in Figure 5a. These maps, generated via CR3BP and BCR4BP analysis, provide initial guesses for higher-fidelity ephemeris analyses.

The two maps in Figure 5 represent the same jettison Δv and TA values during two subsequent revolutions. Thus, the differences between the two maps are caused by the varying Moon angle. The red (recontact), pink (perilune flip), and blue (corner-turn departure) points do not change with varying Moon angle. Conversely, the Moon angle at jettison affects the orientation in the Sun-B_1 frame at departure from the NRHO, and hence the directions that actually yield successful direct heliocentric escape: the green points. Note the large ring of green points with yaw values ranging from about 200º-300º in Figure 5b that is absent in Figure 5a. Some jettison geometries are more favorable than others for finding robust solutions. The jettison maps change significantly as the jettison TA and Δv are varied. For example, two additional maps appear in Figure 6. As in Figure 5, the map in Figure 6a is generated with Δv = 1.7 m/s. However, the jettison in Figure 6a occurs at TA = 160º. The Moon angle at this earlier TA is -87º. The number of jettisons that lead to recontact risk is significantly lower for a maneuver prior to apolune, and the jettison directions that yield energetic departures are very different. Similarly, the jettison map in Figure 6b represents 1 m/s jettisons at TA = 160º. The decreased Δv magnitude again substantially changes the map's characteristics. A further discussion of the evolution of the various regions in the jettison maps with changing TA and Δv magnitude appear in part 1 of this investigation.[7] Jettison maps as pictured in Figure 5 and Figure 6 are used to select jettison directions that yield safe, direct escapes to heliocentric space.

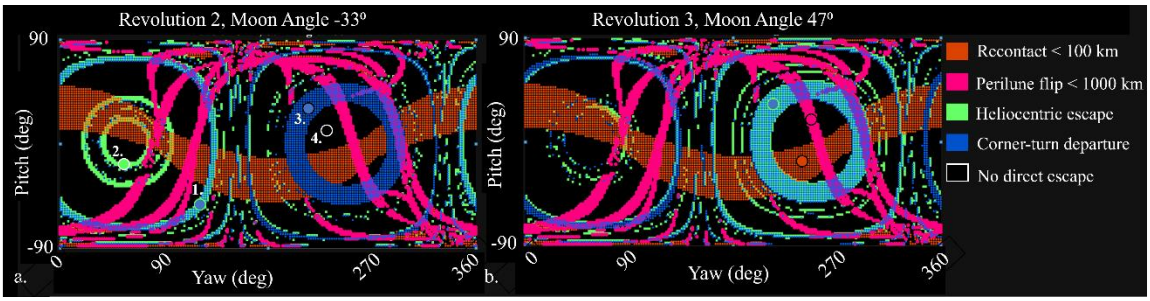

Figure 5. Jettison maps for TA = 200º along revolutions 2 (a) and 3 (b) with Δv = 1.7 m/s

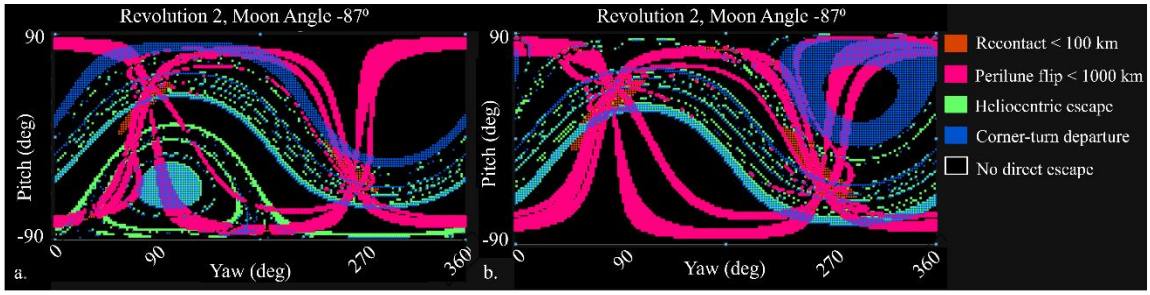

Figure 6. Jettison maps for TA = 160º along revolution 2 with Δv = 1.7 m/s (a) and 1 m/s (b)

Regime 3: Long-term Earth evasion

After successfully achieving escape to heliocentric space, the object enters the third regime defined in this investigation: long-term Earth evasion. An object that departs to heliocentric space does not necessarily avoid returning to Earth. As a concrete example, J002E3,[12] observed in Earth orbit in September 2002, was recognized as the upper stage of the Saturn V rocket from the Apollo 12 mission. Initially in a heliocentric orbit, the upper stage returned to the Earth-Moon vicinity and was recaptured into Earth orbit. After escaping again in June 2003, it may return to the Earth-Moon system in the 2040s. As humanity refocuses on lunar exploration, both crewed and robotic, it is increasingly important to responsibly manage the space environment.[13] Thus, it is important to understand the long-term behavior of objects jettisoned to heliocentric space, whether for science missions or as a disposal destination. One inherent challenge with this third regime is that a disposed object may not be tracked or observed, and if uncontrolled, the attitude and other parameters are unknown. In addition, integration errors over long-term propagations are non-negligible. Thus, specific long-term behavior may not be predictable. Still, understanding the dynamics and predicting what jettison conditions lead to consistent behavior in the presence of expected operational errors is critical.

A spacecraft that escapes the Earth-Moon vicinity through the Sun-B_1 L1 portal is characterized as an internal escape with an osculating heliocentric period shorter than 1 year. Conversely, an L2 escape is exterior to the Earth with a period longer than 1 year. An example of interior and exterior escapes appears in Figure 7. Both samples depart the NRHO via a corner-turn departure after a 15 m/s jettison as illustrated in the Earth-Moon rotating view in Figure 7a, but the departures are from different revolutions along the NRHO. The same trajectories are plotted in the Sun-B_1 rotating frame in Figure 7b. Different epochs and Moon angles at departure yield different post-escape behavior. An L1 interior escape appears in orange, and an L2 exterior escape is plotted in green. Note that exterior escapes move clockwise through the Sun-B_1 frame, while interior escapes move counter-clockwise. Each "bounce" in these plots is approximately 1 year in duration, with the cusps representing perihelia (exterior escapes) and aphelia (interior escapes). Long-term Earth evasion requires that these cusps remain far from the Earth-Moon vicinity. In both the interior and exterior cases, the trajectory avoids returning to the Earth-Moon vicinity, with close approach distances of 7.7 and 8.8 million km respectively. The osculating heliocentric period appears in Figure 7c for each trajectory. After an initial variation in period during the first year after departure from the NRHO, the period levels out until the next close approach of the Earth-Moon system is experienced. Each passage of the Earth-Moon vicinity results in a step in the heliocentric period, which then remains relatively constant while the trajectory is far from the gravitational perturbations of the Earth. The Sun-B_1 Hamiltonian, a measure of energy, appears in Figure 7d for each trajectory.

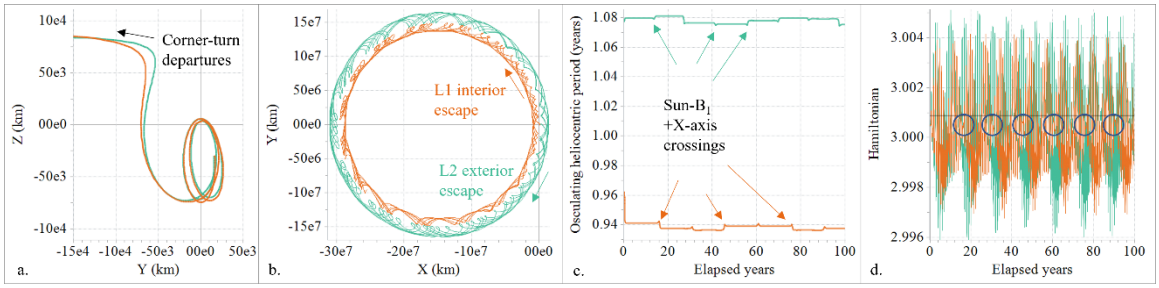

Figure 7. 100-year propagations of interior (orange) and exterior (green) escapes. Earth-Moon rotating view (a), Sun-B_1 rotating view (a), osculating heliocentric period (b), Sun-B_1 Hamiltonian (c).

Both of the examples in Figure 7 successfully evade the Earth-Moon vicinity for 100 years, but many escape trajectories re-approach the Earth after initial escape. One interesting example appears in Figure 8. After an initial interior escape through the L1 portal after a 15 m/s jettison, the trajectory transits the Earth-Moon system approximately 14.5 years after the initial jettison, departing again through the L2 portal. After three exterior revolutions in the Sun-B_1 system, the trajectory again transits the Earth-Moon vicinity, returning to the interior of the solar system though the L1 portal approximately 52.5 years after jettison. Then, 83.5 years after jettison, the trajectory passes again through the L1 portal and is captured by Earth. It remains in Earth orbit for nearly three years before returning to the interior region through L1. The goal of the third regime in this study is to ensure the escape trajectories avoid these close approaches of Earth. Such an example is reminiscent of J002E3, the Apollo 12 upper stage, demonstrates the need for an evasion technique.

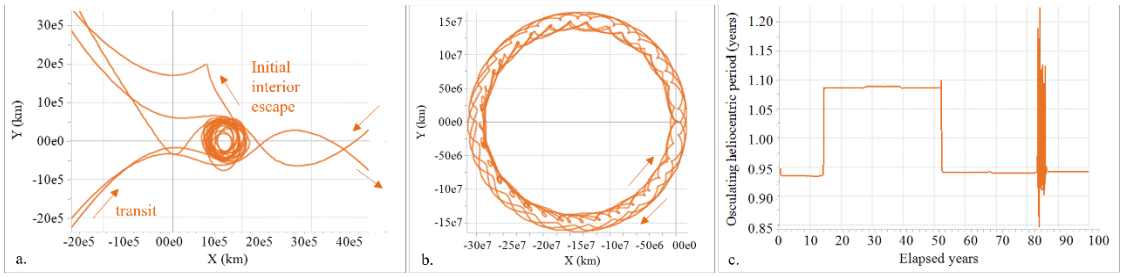

Figure 8. Unfavorable interior escape. Sun-B_1 view (a, b), osculating heliocentric period (c).

One method to forbid the return to the Earth-Moon vicinity is to perform a maneuver to decrease the spacecraft energy and close the Sun-B_1 ZVCs. In the CR3BP, the Jacobi Constant is truly constant, and the ZVCs are time invariant. In the ephemeris model, the Jacobi constant is unavailable, and the Sun-B_1 Hamiltonian is employed as a measure of energy. The Hamiltonian varies over time in the ephemeris model, and the forbidden regions defined by ZVCs also vary. The Hamiltonian as measured at the L1 and L2 libration points is marked in black in Figure 7c; at this scale the two lines are indistinguishable. To ensure the instantaneous ZVC portals are closed at L1 and L2 at any given time, the Hamiltonian must be greater than the L1 and L2 values at that time. Clearly, as propagated in the ephemeris model in Figure 7c, the Hamiltonian of the trajectory varies over time. For both interior and exterior escapes, minimum values are experienced at aphelia, and maximum values at perihelion passages. A large variation in the minimum and maximum Hamiltonian values are observed when the spacecraft is far from Earth, but as the trajectory approaches the Earth-Moon vicinity, the envelope around the Hamiltonian collapses, and the range between the minimum and maximum values is small. These regions corresponding to the close Earth approaches of the interior trajectory in Figure 7a are marked with circles in Figure 7c.

As previously noted, the instantaneous ZVCs must be open for the jettisoned object to initially escape from the Earth-Moon vicinity. In the absence of a targeted flyby to manipulate the Hamiltonian, an additional maneuver after escape from the Earth-Moon vicinity can serve to raise the Hamiltonian to forbid re-entry into the Earth vicinity. For the jettison example from Figure 8, an energy-reducing maneuver is placed at the first perihelion after escape, 296 days after jettison, directed in the anti-velocity direction. In this example, to increase the Hamiltonian sufficiently that it remains entirely above the L2 value throughout the propagation requires a 450 m/s maneuver at the first perihelion. The corresponding Hamiltonian over time and the post-jettison trajectory plotted in the Sun-B_1 rotating frame appear in Figure 9a and b. However, it is not necessary to close the ZVCs at all locations in the Sun-B_1 system; it is only necessary that the instantaneous ZVCs be closed when the trajectory approaches Earth. In this example, a maneuver of 50 m/s applied at perihelion 296 days after jettison is sufficient to raise the Hamiltonian (decrease energy) such that, at the return to the positive Sun-B1 *X*-axis, the instantaneous ZVCs are closed, and the trajectory does not reapproach Earth. The resulting time-varying Hamiltonian and the trajectory plotted in the Sun-B_1 rotating frame appear in Figure 9c and d. The closest approaches to Earth, or the epochs where the trajectory crosses the positive *X*-axis in the Sun-B_1 rotating frame, are marked with circles in Figure 9c. Note that the Hamiltonian at these times remains just above the L2 value represented by the black line. Similar results are observed for exterior escapes with energy-reducing maneuvers placed at the first aphelion after jettison.

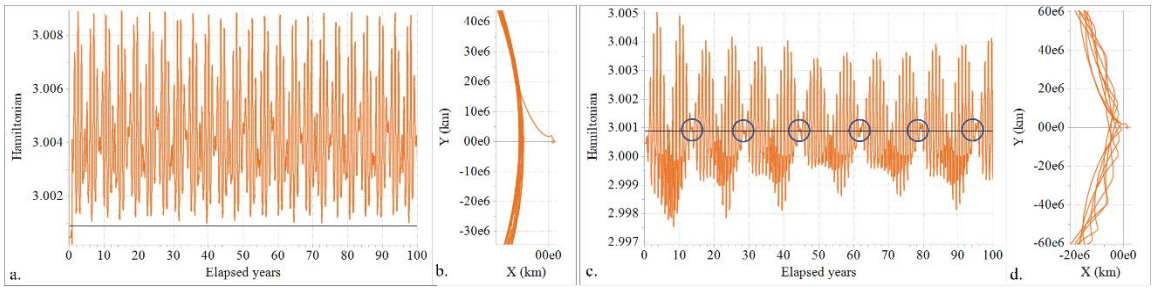

Figure 9. Hamiltonian (a, c) and Sun-B_1 rotating view (b, d) with a 450 m/s energy-reducing maneuver (a, b) and a 50 m/s energy-reducing maneuver (c, d) 296 days after jettison

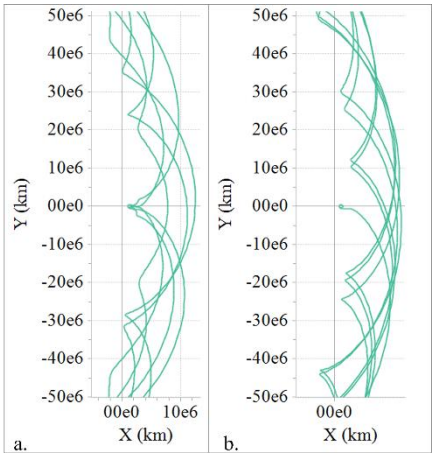

Figure 10. Unfavorable (a) and favorable (b) heliocentric trajectories

While applying an energy-reducing maneuver to close the instantaneous ZVCs is a reliable option to ensure long-term Earth evasion, two challenges are associated with this solution: first, the maneuver may be large compared to the Δv capacity of the spacecraft, and second, the time between initial jettison and the final maneuver may be longer than the operational lifetime of the spacecraft. Thus, a second method is investigated to facilitate long-term Earth evasion that does not require an additional maneuver after initial escape. The second strategy focuses on establishing a resonance in the osculating heliocentric period to prevent perihelion passages near the $+X$ axis in the Sun-B_1 rotating frame for exterior escapes, or similarly, to prevent aphelion passages close to the Earth in the case of interior escapes. An example of an unfavorable and a favorable exterior escape appear in Figure 10. Both cases are jettisoned from TA = 150º along revolution 4 of the baseline NRHO and propagated for 100 years; both cases display resonant behavior. The jettison Δv of 15 m/s in the unfavorable case plotted in the Sun-B_1 rotating frame in Figure 10a is adjusted to 15.3 m/s to produce the favorable case in Figure 10b. Note that the cusps in these exterior escapes, which correspond to perihelion passes, are aligned with the Sun-B_1 $+X$-axis in the unfavorable example in Figure 10a, resulting in repeated close approaches of Earth. Conversely, in the favorable example in Figure 10b, the perihelion passes all remain far from the Sun-B_1 $+X$-axis, and close approaches to the Earth-Moon vicinity are avoided for 100 years. Note the similarity between this favorable pattern and the quasi-periodic trajectory example in Figure 27 of part 1 of this investigation.[7] The goal of this analysis, then, is to identify metrics to reliably achieve the favorable patterns that achieve long-term Earth evasion. The metric of focus in this analysis is the osculating heliocentric period, plotted for interior and exterior examples in Figure 7b. During the first year after jettison, the period changes significantly as the Earth's gravity continues to affect the orbit. The heliocentric period is then relatively constant until the next passage of the Sun-B_1 $+X$ axis near the Earth, when the period generally changes again under the close influence of the Earth. Thus, for each jettison example, the heliocentric period is measured 600 days after jettison, and this instantaneous value, denoted T_{600}, is used to characterize the trajectory behavior. The period, which is slightly more than a year for exterior escapes and less than a year for interior escapes, determines the time required to traverse around the Sun-B_1 system and return to the $+X$ axis near the Earth. In the examples explored here, that time ranges from approximately 13 to 16 years for exterior escapes and about 15 to 20 years for interior escapes. Thus, to ensure Earth evasion for the first ~26-40 years after jettison, only a single return to the Earth vicinity is expected, and avoiding a close approach is relatively simple. For longer durations, however, multiple returns to the Sun-B_1 $+X$ axis occur and selecting an initial jettison that avoids close approaches is more complicated.

To characterize the design space, a relationship between the osculating heliocentric period and the close approach distance is sought. Starting from a jettison maneuver that achieves escape to heliocentric space, the maneuver is adjusted slightly to target varying values of T_{600}. For each resulting trajectory, the close approach range to Earth is recorded and plotted as a function of the targeted T_{600}. For example, the close approach distance as a function of T_{600} for 20-year propagations appears in Figure 11a for interior escapes and in Figure 11b for exterior escapes. Each point is colored according to the time of closest approach. Each plot represents departures from multiple revolutions along the NRHO at TA = 150º. The magnitude of the original jettison Δv for each case is set to 15 m/s, and the direction for each revolution is adjusted to achieve heliocentric escape. Then, for each T_{600} value, the three components of the Δv are each allowed to vary by up to 1 m/s to achieve the specified value of T_{600}. Each colored datapoint in the plots in Figure 11 represents a single heliocentric trajectory such as those appearing in Figure 10. Because the propagation time is set to 20 years, only the first return to the Earth-Moon vicinity is captured. Several observations are immediately notable in Figure 11a-b. First, an oscillation exists in the close approach distance as subsequent perihelion passages approach and then pass the Sun-B_1 $+X$-axis. For exterior escape trajectories, minimum values of close approach occur as each subsequent perihelion aligns with the Sun-B_1 $+X$-axis, and maxima occur when aphelia align with the axis; the converse is true for interior escapes. Second, the time between jettison and the first return to the Sun-B_1 $+X$-axis increases as T_{600} approaches 1 year. For interior T_{600} values greater than

about 0.953 years, the time to complete one revolution around the Sun-B_1 frame is greater than 20 years, so no returns to the Sun-B_1 $+X$-axis are achieved in Figure 11a.

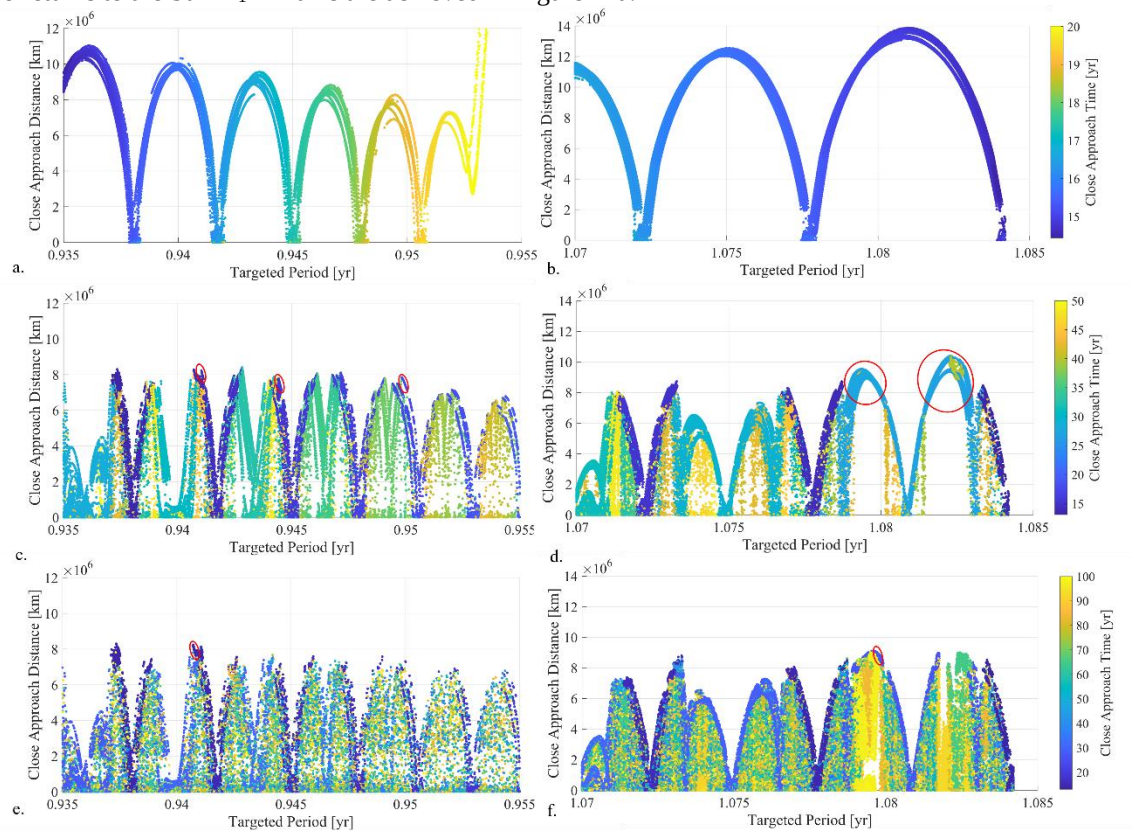

Figure 11. Close approach distance as a function of T_{600} over a 20-year (top), 50-year (middle) and 100-year (bottom) propagations for interior (left) and exterior (right) escapes.

Clearly, to avoid a close passage of Earth at the first return to the Earth-Moon vicinity is simple; many options exist for T_{600} values that evade Earth for 20 years after jettison. As the propagation time is increased to include the second return to the Sun-B_1 $+X$-axis, the patterns become more complex. In this analysis, the only maneuver is the initial jettison from the NRHO, and only a single value of osculating heliocentric period is targeted, the value 600 days after jettison. However, as illustrated in Figure 7b, the osculating period changes each time the Sun-B_1 $+X$-axis is crossed. Thus, the relationship between T_{600} and the close approach distance becomes increasingly indirect as additional axis crossings are added. In Figure 11c-d, the close approach distances for departures from multiple revolutions are again plotted as a function of T_{600}, but the propagation time is increased to 50 years. The simple oscillatory behavior seen in Figure 11a-b is interrupted by a second resonance resulting from the second passage of the Sun-B_1 $+X$-axis. Note that if the maximum approach distance is selected for the first return to the Sun-B_1 $+X$-axis, the second return corresponds to a minimum distance and results in a very close approach, or even a transit or a capture trajectory. For interior escapes, it is challenging to locate a single value of T_{600} that is available as a universal target to ensure Earth evasion for 50 years. For individual revolutions, however, short spans of T_{600} values characterize trajectories that remain far from Earth. Three of these regions are indicated by red circles in Figure 11c. For exterior escapes, however, large spans of T_{600} values yield trajectories that remain far from Earth for 50 years; for example, no Earth approaches within 6 million km are observed for jettisons such that 1.0792 years < T_{600} < 1.0801 years and 1.0792 years < T_{600} < 1.0801 years. These example spans are highlighted with red circles in Figure 11d. Note that interior escapes with 0.935 years < T_{600} < 0.937 years return to the Sun-B_1 $+X$-axis a third time within 50 years, and the third close approach appears for these values in Figure 11c.

When the propagation duration is increased to 100 years, the patterns in the close approach distance are further obscured but not entirely erased. An example appears in Figure 11e-f for interior and exterior escapes, respectively, again colored by the time between jettison and the closest approach. Each subsequent passage

near the Earth-Moon vicinity decreases the close approach distance seen after the first passage in Figure 11a-b, so the T_{600} values that result in trajectories with large minimum close approach distances diminish further with increased propagation time. For interior escapes, a universal favorable span of T_{600} values is not observed. As in the 50-year propagations, however, a small range of T_{600} values identify trajectories that remain far from Earth for a given jettison revolution. For example, the interior trajectory plotted in orange in Figure 7 is generated by targeting T_{600} = 0.94108 years with a 15 m/s jettison from TA = 150º along revolution 2 of the baseline NRHO, and the resulting trajectory does not pass closer than 7.7 million km to the Earth. However, interestingly, a limited region in Figure 11f is identified with T_{600} values that produce trajectories that never return within approximately 8 million km of Earth over 100-year propagations. This region is marked with a red circle in Figure 11f and highlighted in a zoomed-in view in Figure 12. In Figure 12a, the points are colored according to the time past jettison of the closest approach to Earth. At approximately 97 years after jettison, the yellow points indicate targeted periods that yield trajectories that reapproach Earth for some cases. The same datapoints are colored according to the Sun-Earth range at jettison in Figure 12b, and a trend is apparent in the data. For this region of T_{600} values, jettisons when the Earth is closer to perihelion tend to result in closer approaches after about 97 years, while jettisons that occur with the Earth is near aphelion tend to remain far from the Earth at the final crossing of the Sun-B_1 +X-axis in a 100-year propagation. This result highlights the face that the eccentricity of the Earth's orbit and other variations in a high-fidelity force model significantly affect the outcomes of long-term propagations. Though not shown here, it is observed that the favorable patterns in Figure 12 persist through approximately 150 years; shortly after 150 years, a relatively close flyby of the Earth at a radius of about 4 million km disturbs the resonance, and subsequent Sun-B_1 X-axis crossings yield close approaches within 1 million km of Earth. However, despite the variations in the ephemeris model, for the cases simulated here, if the jettison maneuver is tuned to target a heliocentric period 600 days after jettison such that 1.07972 years < T_{600} < 1.07976 years, no returns within 6 million km of Earth are observed for over 100 years. When achievable for a given jettison, these values of T_{600} represent candidate targets for robust longterm heliocentric escape trajectories.

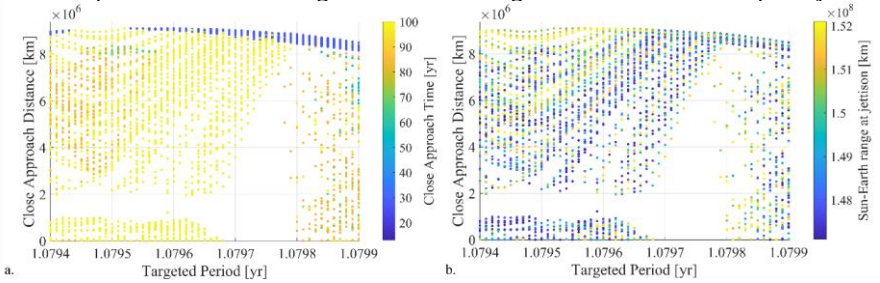

Figure 12. Close approach distance as a function of T_{600} over a 100-year propagation colored by close approach time (a) and Sun-Earth range at jettison (b).

Recall that in this study, the 15 m/s jettison originally targeted to simply achieve escape to heliocentric space is allowed to vary by 1 m/s in each axis to achieve a desired value of T_{600}. The final jettison Δv magnitude for the dataset represented in Figure 11 ranges from 14 m/s to 16.5 m/s. Further opening the allowed variation in the Δv does not generally increase the achievable range of T_{600} values, since a heliocentric escape must first be achieved from the NRHO, and larger variations in Δv are observed to yield Earthbound trajectories. It is also observed that different revolutions along the NRHO yield different achievable ranges of T_{600} for the initial jettison Δv assumptions applied in this study. For example, the exterior escapes from revolution 1 are able to achieve higher values of T_{600} than achieved by exterior escapes from revolution 5 in this simulation. In general, most jettisons from a Moon angle corresponding to revolution 5 as defined in Figure 2 are not able achieve T_{600} = 1.07975 years. Expanding the study to explore indirect escapes such as trajectory 3 in Figure 4 could significantly expand the achievable range of targetable periods.

A single value of T_{600} is observed to offer reliable long-term Earth evasion for exterior escapes when it can be achieved. No similar universal ranges of T_{600} are observed for interior transfers, though for individual jettisons, Earth evasion is achievable. It is important to note that changing the horizon time from 600 days to a different value changes the characteristics of the plots. Other metrics instead of T_{600} may reveal options that are achievable for a wide range of interior or exterior escapes. Other methods entirely, for example, maximizing Earth close approach distance, are also effective; the setup of an optimization problem for long-term Earth evasion is described in the final application in this investigation.

APPLICATIONS: JETTISON FROM THE GATEWAY NRHO

In this investigation thus far, three regimes are defined for successful heliocentric escape: avoiding recontact with the Gateway while departing the Earth-Moon system, achieving escape to heliocentric space, and evading the Earth for extended durations. These three goals must be achieved within the capabilities of the spacecraft and in the presence of realistic operational errors. Three applications are explored: the jettison of modules with maneuvering capability, the jettison of cubesats or objects without maneuvering capability, and the end-of-life disposal of Gateway itself.

Application 1: Module Jettison

The first application considers the jettison of a module that includes a powered bus, such as a logistics module (LM) or a disposable human lander system (HLS) element. In this scenario, after undocking from the Gateway, the LM or HLS element is assumed to perform a ~15 m/s Δv in a specified direction to depart the NRHO for disposal to heliocentric space. It is assumed that the element remains operational for at least two weeks after the initial jettison Δv to clean up dispersions associated with the maneuver. Three jettison locations along the NRHO are explored: TA = 150º, TA = 180º, and TA = 210º. Note that in this study, the jettisons are assumed to be performed directly from the baseline NRHO; in reality, the Gateway will not fly precisely on the baseline trajectory,[14] and finite time and state differences will elapse between module undock and jettison Δv; these specific details are reserved for a future investigation. The jettison maps for the three module jettison locations appear in Figure 13 for departures from revolution 5 along the baseline NRHO (see Figure 2.) Recall that maneuver directions that yield energetic corner-turn departures leading to direct heliocentric escape without recontact risk are identified by regions in the map colored with blue dots overlaid on a green field far from red and magenta points. Note that the jettison location TA = 150º corresponds approximately to the location of maximum corner-turn departures identified in part 1 of the current study.[7] Indeed, it is qualitatively apparent when inspecting the three maps in Figure 13 that the largest blue region appears in Figure 13a. Recall also that while the blue regions that designate corner-turn departures do not depend on Moon angle, the green regions that correspond to direct heliocentric escape change with varying Moon angle. Thus, for each departure TA, a set of 9 maps is generated, one for each Moon angle in the 9:2 resonant sequence. These maps are generated by CR3BP and BCR4BP analysis, but the applications are assessed in the higher fidelity ephemeris force model. To increase the chances of achieving a successful result in the ephemeris model, four initial guesses are selected from each map. Starting with the first guess, a targeter varies yaw and pitch within a 10º box to achieve the condition in Equation 1 that ensures a high-energy departure from the NRHO. If the condition is achieved, the trajectory is classified as either a corner-turn departure or lower departure, and it is checked for direct escape. If a corner-turn direct escape is achieved, the maneuver is selected and the targeter process terminates. If not, the next initial guess is tried, until a corner-turn direct escape is achieved or the four initial guesses are exhausted. If no corner-turn direct escape is achieved, a lower departure direct escape is selected, if available. If no direct escapes are achieved, the revolution is marked as a failed case. In this way, the automated process steps through 500 consecutive revolutions in the NRHO, performing a jettison at the specified TA value each revolution for approximately 10 years from 2020 through 2030. First, the process is completed in the ephemeris force model without considering operational errors. Then, selected trajectories are spot-checked in a Monte Carlo analysis to consider the effects of navigation, maneuver execution, and solar pressure modeling errors.

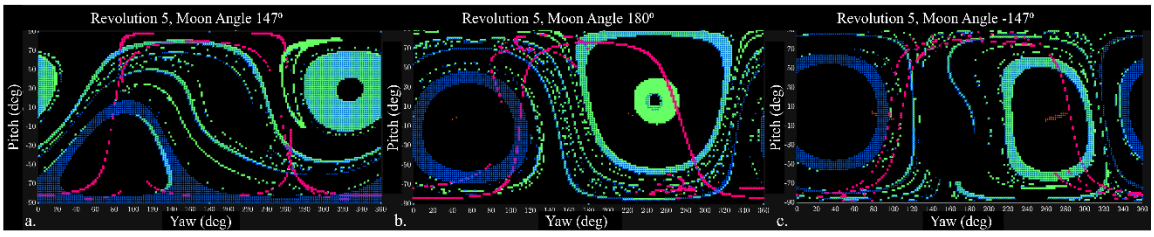

Figure 13. Jettison maps for Δv = 15 m/s from TA = 150º (a), TA = 180º (b), and TA = 210º (c)

The trajectories resulting from this automated process without errors considered appear in Figure 14 for the 500 jettisons from TA = 150º. Of these cases, seven are unable to achieve the target conditions from Equation 1. These seven cases are colored orange in Figure 14. The Earth-Moon rotating view appears in Figure 14a. The corner-turn departures, designated by positive Z values at departure as measured in Earth-

Moon rotating coordinates, are easily distinguished from the 34 lower departures, selected only when corner-turn departures are not achieved. The Sun-B_1 rotating view appears in Figure 14b. Only five cases remain Earthbound, all of which fail to target the high-energy departure condition; the other 495 trajectories achieve direct heliocentric escape. The range between the Gateway and the jettisoned element appears in Figure 14c. All 500 jettison trajectories depart the NRHO without re-entering the 100 km keep-out sphere or experiencing a flip in the range pattern at perilune within 1000 km. For departures from TA = 150º with a Δv magnitude of 15 m/s, the automated process is successful.

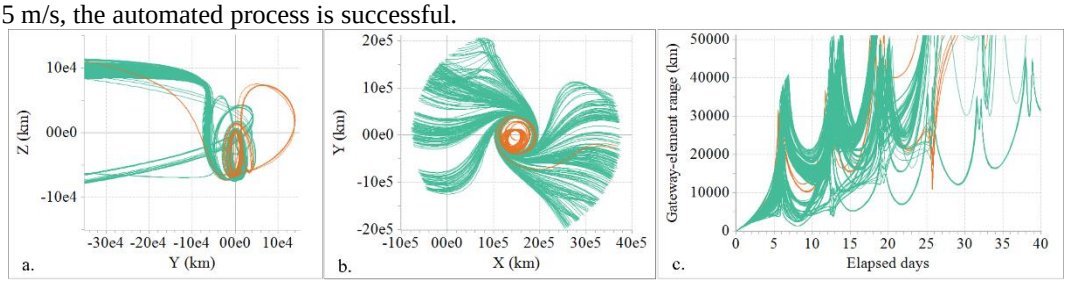

Figure 14. Earth-Moon rotating view (a), Sun-B_1 rotating view (b), and Gateway-element range over time for 500 jettisons from TA = 150º with Δv = 15 m/s

As predicted by the jettison map for departures from TA = 180º in Figure 13b, which has fewer broad regions of favorable blue-green overlap to provide robust initial guesses, the results from this location include more failed cases. Of the 500 jettisons performed at TA = 180º, 15 fail to target, and 21 either remain Earthbound or achieve an indirect escape to heliocentric space after one or more revolutions around the Earth. Two cases experience a flip in the range at perilune, each reaching a range under 800 km approximately 10 days after jettison. Despite the more challenging jettison location, 477 of the 500 jettison trajectories achieve the desired escape conditions, though 93 are unable to target corner-turn departures and instead resort to lower departures. The jettisons from TA = 210º are also highly successful, with only 8 jettisons that fail to target Equation 1. Only three of these remail Earthbound. One targeted case experiences a flip in the range pattern at perilune, with a close approach of 603 km about 1 week after jettison. The majority of the jettisons achieve corner-turn departures; 43 cases revert to lower departures. For all three of the jettison locations sampled with a 15 m/s maneuver, the jettison maps provide excellent initial guesses to achieve desired results in the higher fidelity ephemeris model. Though it is not shown here, it is expected that some or all of the cases that fail to target in the automated process may be successful with manual intervention. However, due to the Sun-Earth geometry, it may not be possible to achieve a corner-turn departure that directly escapes to heliocentric space at every possible jettison epoch.

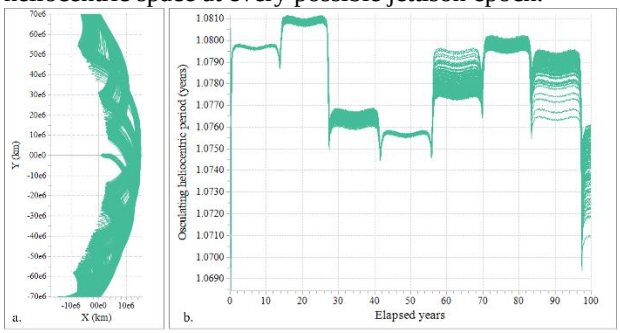

Figure 15. External escaping trajectories successfully evade Earth for 100 years. Sun-B_1 rotating view (a) and osculating heliocentric period (b).

Next, long-term Earth evasion is explored for the 15 m/s jettisons from TA = 150º. For each jettison that achieves an external escape to heliocentric space, the jettison maneuver is adjusted to target T_{600} = 1.07975 years, and the resulting trajectory is propagated for 100 years. In this simulation, 229 of the 500 jettisons sampled escape through L2 and achieve exterior heliocentric orbit. Of the 229 exterior escapes, 176 jettison maneuvers are successfully adjusted to target the desired value of T_{600}. In the set of 176 trajectories that achieve the targeted T_{600} value, the closest approach to the Earth occurs for a jettison in 2030, with a distance of 6.3 million km reached 97 years after jettison. The closest approach within the first 90 years after jettison passes within 8.6 million km of the Earth 27 years after jettison. A zoomed-in view of the 176 trajectories plotted in the Sun-B_1 rotating frame appears in Figure 15a. Note the consistent escapes through the Sun-B_1 L2 portal and the consistent evasion of the Earth vicinity throughout the dataset. The osculating heliocentric period values over time appear in Figure 15b. Note that the period follows a consistent pattern for each trajectory that successfully achieves the targeted T_{600} value. Note also that the spread in osculating period becomes broad after the Sun-B_1 $+X$-axis crossing after 97 years; the favorable, predictable resonance is likely to be

lost for longer propagations. It is noted that most of the 53 jettisons that fail to target the desired heliocentric period originate from a Moon angle corresponding to that of revolution 5 (see Figure 2), which, as mentioned previously, is rarely able to achieve a T_{600} value as high as 1.07957 years. It is expected that with manual intervention, many of these failed cases could find a successful outcome for long-term heliocentric evasion.

Thus far, the analysis for the 15 m/s jettison cases neglects to consider realistic operational errors. It is important to understand whether proposed jettison solutions are robust when such errors are included in the simulation. In this study, navigation, maneuver execution, and solar radiation pressure (SRP) modeling errors are included as summarized in Table 1. For simplicity, the Gateway is assumed to be uncrewed for the duration of the simulations. The Gateway is maintained in its orbit during the simulation; SRP area error is updated at perilune each revolution, while Cr error is updated at the start of every trial. Navigation errors are and maneuver execution errors are applied at each orbit maintenance maneuver (OMM).[15] For the jettisoned module, a larger navigation error is applied, as it is assumed that the spacecraft undocks just prior to the jettison maneuver, adding uncertainty to the pre-jettison state. An execution error is applied to the jettison itself, and SRP area and Cr modeling errors are applied at jettison.

Table 1. Errors applied in Gateway and jettison simulations

	Error Type	3σ: Gateway	3σ: module at jettison	3σ: module at cleanup	3σ: cubesat at jettison
SRP Errors	SRP Area Error %	30	30	30	30
	SRP Cr Error %	15	15	15	15
Navigation Errors	Position Error (km)	1	10	1	10
	Velocity Error (cm/s)	1	10	1	10
Maneuver Execution Errors	percent magnitude %	1.5	2	2	10
	fixed magnitude (mm/s)	1.42	-	-	-
	direction (deg)	1	1	1	5

The three regimes are assessed in the Monte Carlo simulations to evaluate success in each portion of the problem: whether the jettisoned module departs the NRHO without risking Gateway recontact, whether the module successfully escapes to heliocentric space, and whether the module evades Earth for 100 years after jettison. A representative case is included here; a comprehensive study remains future work. The selected example is a corner-turn departure that exits the Sun-B_1 L2 portal. The initial 15 m/s Δv is adjusted to 14.8 m/s to successfully target T_{600} = 1.07975 years from TA = 150º along the first revolution in the baseline NRHO. With errors applied to the Gateway and the jettisoned module as specified in Table 1, 1000 Monte Carlo trials are executed, and the results appear in Figure 16. The Earth-Moon rotating view of the departing trajectory appears in Figure 16a. While the dispersions in the trajectory are visually apparent, it is also clear that the corner-turn geometry is maintained by each trajectory. When the trajectories are viewed in the Sun-B_1 rotating frame, as in Figure 16b, it is clear that all 1000 trials successfully exit through the Sun-B_1 L2 portal to heliocentric space. During the departure, each sample trajectory remains far from Gateway, as is apparent in the plot of Gateway-module range in Figure 16c. Thus, this jettison example is robust in the first two regimes: it successfully departs the NRHO without recontact risk, and subsequently successfully escapes to heliocentric space. Although the results are not shown here, it is observed that this jettison example remains robust in the first two regimes for jettison errors of 10% (3σ) in magnitude or if T_{600} is not targeted after Equation 1 is satisfied. It is noted that a similar jettison from revolution 10 produces a lower-departure geometry; this example from revolution 10 is robust for regimes 1 and 2 with errors as outlined in Table 1 if the favorable value of T_{600} is targeted. However, this lower-departure case fails to reliably depart the NRHO without recontact risk or to escape the Earth-Moon vicinity if T_{600} is not targeted or if the jettison magnitude errors are increased to 10% (3σ).

The third regime is more complicated due to the high sensitivity of the long-term heliocentric trajectories[7] and the extended duration of the propagations. The dispersions apparent in the escaping trajectories in Figure 16b suggest that the targeted heliocentric period may not be achieved. Indeed, when the 1000 Monte Carlo trials from Figure 16 are extended to a 100-year propagation, the resulting trajectories display unpredictable behavior. The desired patterns from Figure 10b and Figure 15 are lost as a result of the operational errors. The results of the simulation appear in Figure 17. The trajectories are plotted in a zoomed-in Sun-B_1 rotating view in Figure 17b and in a zoomed-out view in Figure 17c, with the error-free nominal case overlaid in black. Of the 1000 trials, 37 trajectories transit the Earth-Moon vicinity at least once to become interior orbits, and 16 trials impact Earth. The osculating heliocentric period as a function of time for each trial appears in Figure 17d. Until the first return to the Sun-B_1 +X-axis 14 years after jettison, the

period is relatively consistent across the dataset. However, the first close approach of the Earth differs sufficiently from one trial to the next that all predictable behavior is lost for the rest of the 100-year propagation. Although the error-free trajectory displays desirable behavior, under the influence of realistic operational errors, the desired long-term behavior is not achievable with a single jettison maneuver.

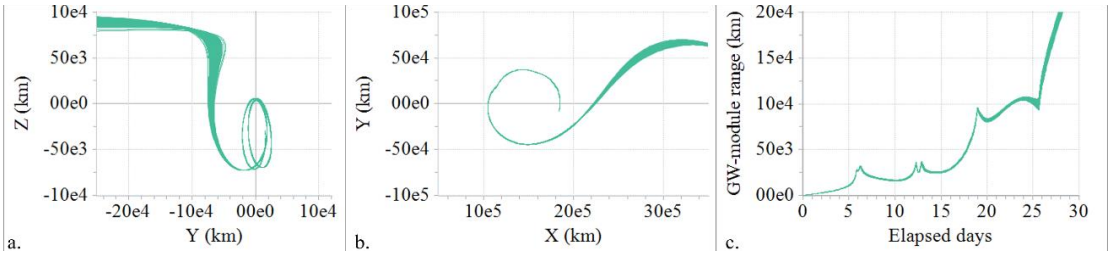

Figure 16. Earth-Moon rotating (a) and Sun-B_1 rotating (b) views of 1000 jettisons; Gateway-module range over time (c).

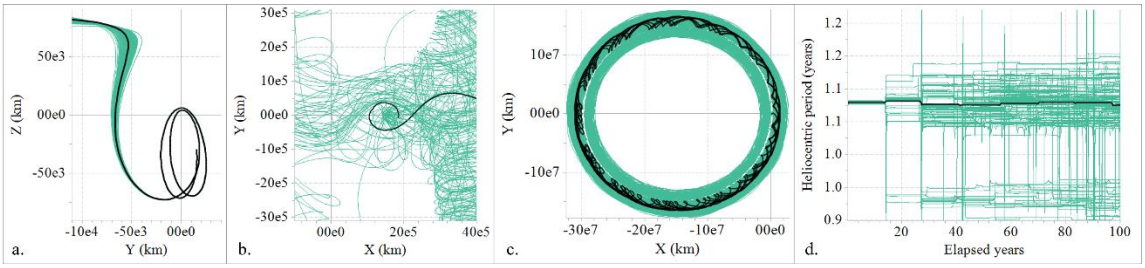

Figure 17. Earth-Moon (a) and Sun-B_1 (b, c) rotating views and osculating heliocentric period (d) for 250 long-term propagations of escaping trajectories without a cleanup burn.

To mitigate the effects of the dispersions at jettison that disturb the desired outcomes, a cleanup burn is designed 15 days after the initial jettison. This operations concept assumes that the jettisoned module is controlled and tracked until cleanup execution. The cleanup burn is initialized with a Δv of zero in each component and targets the same value of T_{600} at the same downstream epoch as the initial jettison. The 1000-trial Monte Carlo simulation is repeated with the cleanup burn implemented. Errors are applied at the cleanup burn in addition to the initial jettison: navigation errors, SRP modeling errors, and cleanup execution errors are specified in Table 1. The navigation error is assumed to be smaller than in the initial jettison since no significant events are assumed to occur in the 2 weeks between initial jettison and cleanup. The resulting cleanup burn is very effective at mitigating the jettison dispersions. With an initial jettison Δv of 14.8 m/s, the cleanup burn magnitude ranges from 0 to 3.7 m/s, with a mean value of 0.9 m/s. Results from the first 250 trials appear in Figure 18. In the Earth-Moon rotating view in Figure 18a, the trajectories are colored orange after the cleanup burn. Note the tighter pattern in the corner-turn geometry as compared to the trajectories without cleanup burns in Figure 17a. A zoomed-in Sun-B_1 rotating view appears in Figure 17b. Note that the resonant pattern is maintained by all 250 trajectories; the full Sun-B_1 rotating view appears in Figure 17c, and the expected patterns are maintained around the Sun-B_1 system. The osculating heliocentric period appears in Figure 17d. The period changes in a step pattern each time the module passes near the Earth, but the favorable pattern in period observed in Figure 15b is maintained by each trajectory.

The close approach distance for each trial as function of the close approach time past jettison for the two cases appears in Figure 19; each figure contains 1000 datapoints representing 1000 dispersed trajectories. Without a cleanup maneuver in Figure 19a, the close approaches occur as soon as first return to the Earth vicinity approximately 14 years after jettison; in fact, one trial impacts the Earth at the first return. The times of close approach disperse further with each passage of the Sun-B_1 $+X$ axis. Of the 1000 trials, 125 trajectories pass within the orbital radius of the Moon, and 218 pass within 1 million km of Earth. When the cleanup burn is included in the simulation, the behavior of the post-jettison trajectories is predictable over 100 years. As illustrated in Figure 19b, the closest approaches to the Earth remain greater than 8 million km and occur either 27 or 97 years after jettison. While these results demonstrate robust behavior in regime 3 for this example, it is important to note that they represent a single sample jettison with simulated errors as defined

in Table 1. Similar results are observed for other sample jettisons, but a comprehensive study, as well as a sensitivity study to error levels, remains forward work.

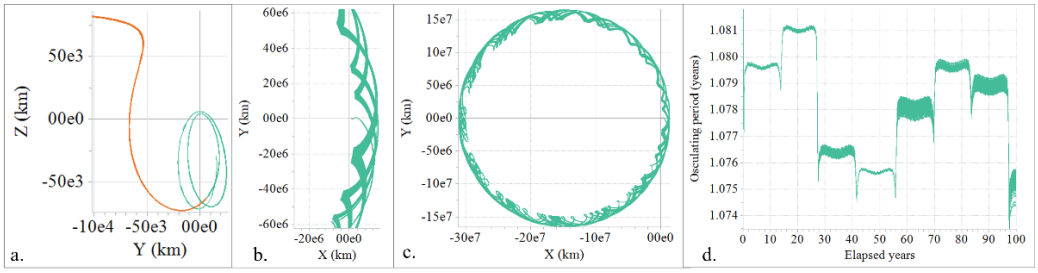

Figure 18. Earth-Moon (a) and Sun-B$_1$ (b, c) rotating views and osculating heliocentric period (d) for 250 long-term propagations of escaping trajectories with a cleanup burn 15 days after jettison.

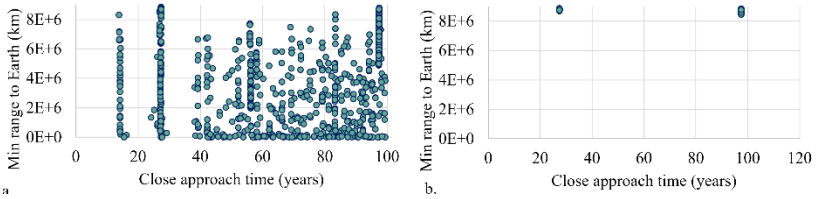

Figure 19. Minimum range to Earth as a function of close approach time without (a) and with (b) a post-jettison cleanup burn for 1000 trials.

Application 2: Cubesat Jettison

The second application simulates the jettison of a passive object via a spring mechanism. Such an object could be a cubesat without propulsive capability, a docking cover for a module, or another unwanted object jettisoned from an arriving or departing vehicle. In this case, the jettison Δv is lower; a value of 1.7 m/s is selected for this example. The smaller Δv in this case results in a slower departure from the NRHO with more revolutions around the Moon in which errors multiply prior to departure and escape. Larger errors on the jettison itself are assumed, as specified in Table 1. In addition, no cleanup burn is possible for the passive object after jettison. Immediately, it is noted that long-term evasion is not possible given the assumptions in this study- since a faster, more accurate jettison in Application 1 fails to evade Earth for more than 14 years without a cleanup burn, clearly a slower, less accurate jettison is not capable of long-term evasion unless different methods, not identified here, are employed. Thus, this example focuses on regimes 1 and 2, safe departure from the NRHO and escape to heliocentric space. To simulate an object jettisoned near arrival or departure of a vehicle taking a fast transfer from Earth,[16] TA values of 160º and 200º are selected. The jettison maps for these two scenarios appear in Figure 5 and Figure 6a. As described in Application 1, four initial guess options are selected from the jettison maps for each TA-Moon angle pair. Note that for some Moon angles, the bands of overlaid green and blue points representing corner-turn departures that yield immediate escape to heliocentric space are quite narrow as compared to the 15 m/s maps in Figure 13, indicating that application in the ephemeris model may be more challenging. As in application 1, a jettison is simulated at the specified TA value for the first 500 revolutions in the baseline NRHO. The results for 1.7 m/s jettisons from TA = 150º appear in Figure 20. Solutions that successfully converge on the energetic-escape condition in Equation 1 are colored green, while solutions that fail to converge are plotted in orange. In this simulation, 475 of the 500 jettison attempts successfully target the condition in Equation 1. All but 26 cases directly escape to heliocentric space; 24 of the Earthbound jettisons fail to converge. The other two Earthbound cases achieve high-energy escapes with poor orientation. These two Earthbound trajectories are visible in the results and are marked with arrows in the Sun-B$_1$ view in Figure 20; while they do not qualify as direct escapes here, both likely escape indirectly in a longer propagation. Corner-turn departures are achieved by 386 of the escaping trajectories; the other 88 are lower departures. Of the 474 direct escapes, 228 escape through the Sun-B$_1$ L2 portal, the rest through L1. Flips in the Gateway-cubesat range are observed in 19 of the jettison trajectories, primarily 11-18 days after jettison. The closest approaches in the flip trajectories are 53 km and 99 km, both occurring 12 days after jettison. Four jettisoned objects impact the Moon. Similar results are observed for 1.7 m/s jettisons simulated at TA = 200º along the first 500 revolutions in the baseline NRHO. In this case, all 481 of the converged cases escape, and all 19 of the jettisons that fail to target

Equation 1 remain Earthbound. Corner-turn departures are achieved by all but 71 of the escaping trajectories; the rest employ lower departures. One lunar impact is observed, and 19 trajectories experience flips in the range at perilune; 14 of these trajectories return within 300 km of Gateway approximately 20 days after jettison.

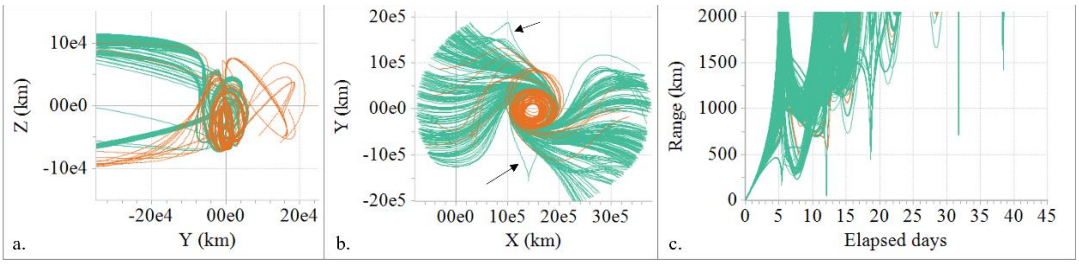

Figure 20. Earth-Moon rotating view (a), Sun-B_1 rotating view (b), and Gateway-cubesat range over time for 1.7 m/s jettisons from TA = 160º for 500 consecutive revolutions

The 500 jettisons in Figure 20 are executed without considering errors. To assess their robustness in a more realistic scenario, the errors as defined in Table 1 are applied and 1000 Monte Carlo trials are run to spot-check several jettisons. The corner-turn departure resulting from a 1.7 m/s jettison from TA = 150º along revolution 1 appears in Figure 21a-b. The error-free trajectory is plotted in black, and the 1000 perturbed trials appear in green. Noticeable variations appear in both the departure from the NRHO and the eventual escapes from the Earth-Moon vicinity. Of the 1000 trials, only two remain Earthbound, and one escapes through the L1 portal. Eighteen are classified as lower departures, and 16 experience flips in the range at perilune below 1000 km approximately 31 days after jettison, but none approach the Gateway closer than 900 km. The 1000-trial simulation is repeated for the corner-turn departure starting from revolution 2, again at TA = 160º, that nominally results in an L1 escape. In this case, 19 of the 1000 trials remain Earthbound, the rest achieve direct heliocentric escape, one though L2 and the rest via the L1 portal.

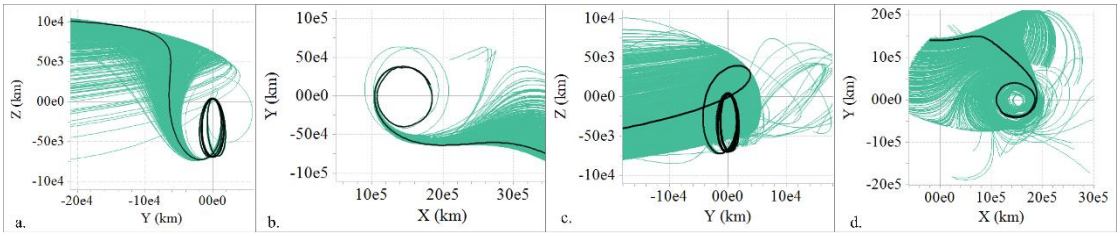

Figure 21. Earth-Moon and Sun-B_1 rotating views for corner-turn (a,b) and lower (c,d) departures in a 1000-trial simulation. Jettisons from TA = 160º with Δv = 1.7 m/s.

Next, a lower departure is investigated. As noted, lower departures tend to be less robust to errors as compared to the prioritized corner-turn departures. The selected example departs from TA = 160º along revolution 8 of the baseline NRHO. The trajectories from the 1000-trial Monte Carlo simulation appear in Figure 21c-d, with the error-free case overlaid in black. With the lower departure case, 556 of the 1000 trials remain Earthbound, while 444 directly escape to heliocentric space. In the presence of errors, this jettison yields unpredictable behavior. Similar results are observed with other lower departure cases.

Finally, a trajectory that experiences a flip in the Gateway-cubesat range at perilune is investigated. The 1.7 m/s jettison from TA = 160º along revolution 187 results in a close approach of 53 km 12 days after jettison when no errors are considered. Of 1000 Monte Carlo trials, all but 5 continue to experience flips in the Gateway-cubesat range at perilune 12 days after jettison, with a minimum range of 9 km for the closest approach case. A zoomed-in view of the Gateway-Cubesat range curves appears in green in Figure 22, with the nominal no-errors case overlaid in black.

It is important to note that the Monte Carlo simulations included here contain results for only a handful of representative examples. A thorough characterization of the design space and a sensitivity analysis to errors is forward work. It is noted that improved results may be obtained with a more accurate jettison; it is also noted that specific perturbations such as outgassing are not included here and may need to be added for specific applications. Additionally, it is likely possible to improve the results for a specific departure epoch by tuning the automated solution generated here to find the most robust trajectory for a given date. The

examples thus far focus on a single jettison TA for each dataset. In practice, datasets are frequently generated with a range of TA values based on specific mission opportunities over a range of epochs. The methods outlined here have been successfully used to yield high success in an automated analysis of datasets covering a range of jettison TA values by creating bins for TA as well as Moon angle and selecting the closest initial guess for each specific jettison opportunity.

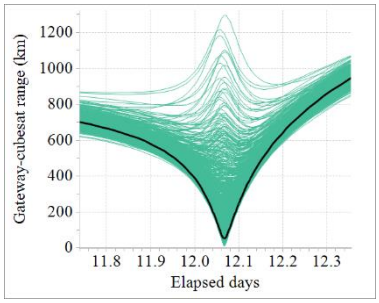

Figure 22. Gateway - cubesat range in a 1000-trial simulation with a range flip at perilune

The methods outlined in this study offer an alternative to the "green zones" for cubesat deployment described in a previous investigaton.[6] Four green zones in jettison location, direction, and magnitude defined in this 2022 study offer safe departure from the NRHO, or robust behavior through regime 1, for an object jettisoned from any revolution along the baseline NRHO. However, of the four identified TA-direction- magnitude sets, only the two green zones defined after apolune yield high-energy departures that offer escape to heliocentric space for some of the defined ranges of Δv magnitude and for certain jettison epochs. The two green zones defined prior to apolune yield low-energy, Earthbound trajectories for their full range of TA and Δv magnitude. The methods described here using jettison maps identify additional jettison options to achieve safe NRHO departure while allowing access to a wider variety of destinations.

Application 3: Gateway End-of-Life Disposal

Heliocentric orbit has been considered as a potential disposal orbit for the Gateway itself at its operational End-of-Life (EOL). Such a disposal would use the Gateway low-thrust electric propulsion system to depart the NRHO on a trajectory that would directly enter heliocentric orbit and not return to the Earth-Moon system for at least 100 years. To that end, two optimization methods have been developed to design potential heliocentric disposal trajectories. The first method directly maximizes the closest Earth range achieved over the 100 years following disposal to design a nominal disposal trajectory that stays as far away from Earth as possible. The second method incorporates operational uncertainty into the optimization objective in order to design a nominal disposal trajectory that not only stays far away from Earth, but is also robust to imperfect execution. Both methods use the full ephemeris model with point mass gravity for the Earth, Moon, Sun, and all planets, and solar radiation pressure. A brief overview of each method is presented along with one example EOL disposal trajectory generated from each as shown in Figure 23 and Figure 24.

The first approach, referred to here as the Range method, uses NASA's Copernicus[17] to design the disposal as a single shooting direct optimization problem beginning in the Gateway reference NRHO. The initial epoch, duration and direction of a single low thrust finite burn serve as optimization variables. The low-thrust Δv is bounded to be less than 5 m/s. To encourage a more direct departure, a constraint is applied to enforce a minimum Earth range of 1.5 million km after 395 days. After 395 days, additional segments are added every 100 days for 100 years with the Earth range at each segment boundary added as part of the objective function. The instantaneous single minimum value of the 100 Earth range objectives is maximized using SNOPT[18]. The numerical challenges introduced by the potentially discontinuous formulation of the objective function and the sensitive nature of the departure dynamics are overcome using a parallel monotonic basin hopping wrapper around Copernicus.[19]

The second approach, referred to here as the Robust method, is used to design a nominal disposal trajectory that stays away from Earth for 100 years in the nominal case and is also robust to dispersions applied at some delivery interface to that nominal disposal trajectory. A similar set of departure optimization variables are used as in the first approach, but in this case the trajectory is propagated using NASA's General Mission Analysis Tool (GMAT). After the finite burn is applied, the nominal trajectory is propagated for 60 days, at which time a series of 20 branching trajectories are spawned from the nominal. The initial state of each branching trajectory is randomly dispersed using normal distributions with zero mean, 3-sigma values of 1 km in position, 0.1 km/s in velocity, and 30% in both solar radiation pressure area and coefficient of reflectivity. The applied dispersions are meant to represent operational delivery errors and uncertainty that would realistically remain after a final targeted delivery to the nominal disposal trajectory. After propagating the nominal and dispersed trajectories for 100 years, statistics on the resultant minimum Earth ranges achieved over 100 years are compiled. The objective for this method is to maximize the mean-minus-3-sigma Earth range ($\mu - 3\sigma$). The numerical difficulty presented by the stochastic objective function and the

additional propagations are overcome by wrapping GMAT with a gradient-free, parallelized extended ant colony optimization algorithm via pygmo[20].

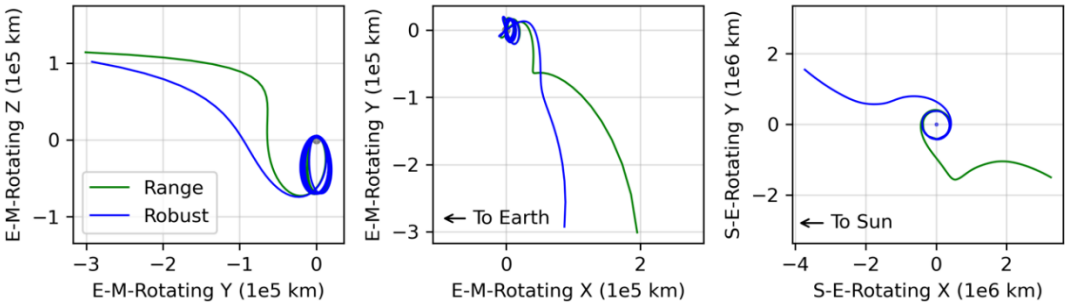

Figure 23. Example Range (green) and Robust (blue) method disposal trajectories shown Y-Z Earth-Moon rotating view (left), X-Y Earth-Moon rotating view (middle), Sun-Earth rotating view (right)

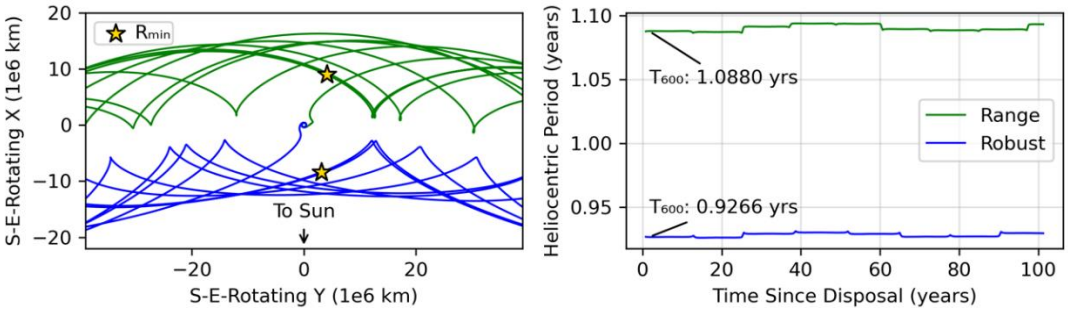

Figure 24. Example Range (green) and Robust (blue) method disposal trajectories in Sun-Earth rotating view (left) and their heliocentric orbit period (right)

Figure 25 provides a demonstration of the effectivity of the Robust method in improving disposal reliability with uncertainty compared to the Range method. For each nominal trajectory, dispersions are applied for varying delivery times after departure (x) and nominal dispersion multiple (y). The contours show the $\mu - 3\sigma$ earth range achieved for the Range method on the left, and Robust method on the right. A total of 40,000 propagations were used to generate each plot. The Robust method trajectory is able to reliably stay well outside the Earth sphere of influence (~10^6 km) for 100 years even with as much as 10-times the nominal delivery dispersions. Further, the Robust method trajectory can accommodate the larger delivery dispersions earlier in the disposal. The Range method trajectory is able to stay further away from Earth in the nominal case, (9.8 vs. 8.9 million km) but is shown to not be nearly as robust when delivery dispersions are included. In either case, the dispersions applied before the final perilune passage result in unreliable disposal behavior with $\mu - 3\sigma$ Earth ranges inside the sphere of influence.

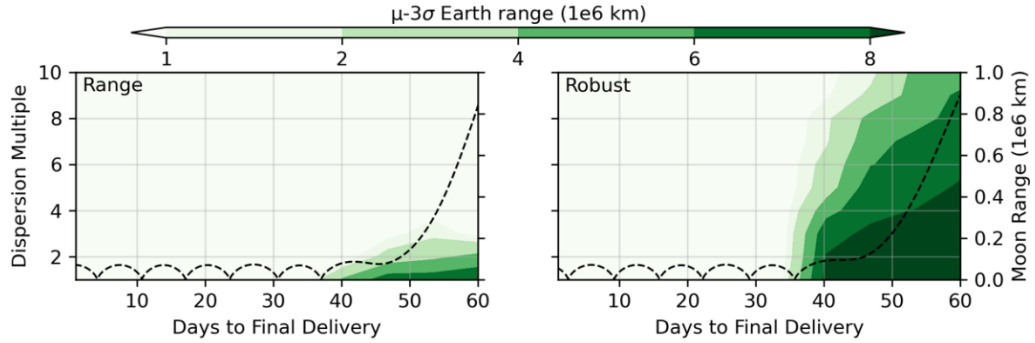

Figure 25. Contours of $\mu - 3\sigma$ Earth range achieved as a function of time to final delivery and multiple of the nominal dispersions. The nominal range to the moon is plotted on the second y-axis.

In summary, both methods presented are successful in designing nominal heliocentric disposal trajectories that maintain adequate distance from Earth over 100 years. Maximizing the resultant minimum

range is a straightforward approach to designing a well-behaved nominal trajectory, but the addition of a statistical component to the optimization objective can improve the reliability of the disposal under realistic operational uncertainty.

CONCLUDING REMARKS

This study demonstrates methods to design jettison conditions that yield safe departure from the Gateway and successful escape to heliocentric space, including long-term Earth evasion under some circumstances. Jettison maps are employed to identify maneuver location/direction/magnitude sets that enable NRHO departure without conjunction risk to the Gateway. Two departure geometries are observed to yield high-energy trajectories: corner-turn geometries are observed to be more robust to errors than lower departures. By targeting specific values of osculating heliocentric period, long-term Earth evasion can be achieved in some cases, though a cleanup burn is necessary to mitigate dispersions and preserve desirable resonances. Techniques are applied to module disposal, cubesat deployment, and Gateway end-of-life scenarios. While an automated process is developed to identify favorable jettisons in many cases, individual jettison trajectories have unique characteristics that are worth exploring. A thorough analysis of the design space considering specific operational constraints should be completed for any given application.

ACKNOWLEDGMENTS

The authors would like to thank Randy Eckman, Damennick Henry, Dale Williams, Paul Lane, Benjamin Asher, David Lee, Alexander Apyan, and Yusef Johnson for insightful discussions. The authors recognize extensive contributions by Kenza Boudad that laid the groundwork for the analysis in this paper.

REFERENCES

[1]Lehnhardt, E. H. and S. M. Fuller, "Gateway Program Progress and Overview," 73rd International Astronautical Congress, Paris, France, October 2022.

[2] Zimovan, E., K. C. Howell, and D. C. Davis, "Near Rectilinear Halo Orbits and Their Application in Cis-Lunar Space," 3rd IAA Conference on Dynamics and Control of Space Systems, Moscow, Russia, May-June 2017.

[3] Boudad, K. K., D. C. Davis, and K. C. Howell, "Disposal Trajectories from Near Rectilinear Halo Orbits," AAS/AIAA Astrodynamics Specialists Conference, Snowbird, Utah, August 2018.

[4] Davis, D. C., K.K. Boudad, and K.C. Howell, "Disposal, Deployment, and Debris in Near Rectilinear Halo Orbits," AAS/AIAA Space Flight Mechanics Meeting, Maui, Hawaii, January 2019.

[5] Davis, D. C., K. K. Boudad, R. J. Power, and K. C. Howell, "Heliocentric Escape and Lunar Impact from Near Rectilinear Halo Orbits," AAS/AIAA Astrodynamics Specialists Conference, Portland, Maine, August 2019.

[6] Davis, D. C., E. M. Zimovan-Spreen, R. J. Power, and K. C. Howell, "Cubesat Deployment from a Near Rectilinear Halo Orbit," AIAA/AAS Spaceflight Mechanics Meeting, San Diego, California, January 2022.

[7] Scheuerle, S. T., D. C. Davis, E.M. Zimovan-Spreen, B. P. McCarthy, and K. C. Howell, "Jettison and disposal from Near Rectilinear Halo Orbits Part 1: Theory," AAS/AIAA Astrodynamics Specialists Conference, Big Sky, Montana, August 2023.

[8] McGuire, M. L., S. L. McCarty, D. J. Grebow, T. A. Pavlak, S.N. Karn, K.S. Ponnapalli, D. C. Davis, and K. Hack, "Overview of the Lunar Transfer Trajectory of the Co-Manifested First Elements of NASA's Gateway," AAS/AIAA Astrodynamics Specialists Conference, Virtual, August 2021.

[9] Zimovan-Spreen, E. M., S.T. Scheuerle, B. P. McCarthy, D. C. Davis, and K. C. Howell, "Baseline Orbit Generation for Near Rectilinear Halo Orbits," AAS/AIAA Astrodynamics Specialists Conference, Big Sky, Montana, August 2023.

[10] Lee, D.E., "Gateway Destination Orbit Model: A Continuous 15 Year NRHO Reference Trajectory," NASA Johnson Space Center White Paper, August 20, 2019.

[11] Phillips, S. M. and D. C. Davis, "Cloud Computing Methods for Near Rectilinear Halo Orbit Trajectory Design," AAS/AIAA Astrodynamics Specialists Conference, Portland, Maine, August 2019.

[12] Jorgensen, K., A. Rivkin, R. Binzel, R. Whitely, C. Hergenrother, P. Chodas, S. Chesley, and F. Vilas, "Observations of J002E3: Possible Discovery of an Apollo Rocket Body," AAS Planetary Sciences Meeting #35, Monterrey, California, September 2003.

[13] Joffre, E., S. Ventura, D. Davis, S Lizy-Destrez, P. Guardabasso, "Management of Lunar Orbits, Session 3- Towards an Environment-Friendly Approach to Lunar Exploration," AAE International Conference on Space Exploration, Turin, Italy, May 2023.

[14] Davis, D. C., B. P. McCarthy, and E. M. Zimovan-Spreen, "Perturbations and Recovery in the Gateway Near Rectilinear Halo Orbit," AAS/AIAA Spaceflight Mechanics Meeting, Austin, Texas, January 2023.

[15] Davis, D. C., S. T. Scheuerle, D. A. Williams, F. S. Miguel, E. M. Zimovan-Spreen, and K. C. Howell, "Orbit Maintenance Burn Details for Spacecraft in a NRHO," AAS/AIAA Astrodynamics Specialist Conference, Charlotte, North Carolina, August 2022.

[16] Whitley, R. J., D.C. Davis, L.M. Burke, B. P. McCarthy, R.J. Power, M. L. McGuire, and K. C. Howell, "Earth-Moon NRHO and Butterfly Orbits for Lunar Surface Exploration," AAS/AIAA Astrodynamics Specialists Conference, Snowbird, Utah, August 2018.

[17] Williams, J., J. S. Senent, C. Ocampo, R. Mathur, and E. C. Davis, "Overview and software architecture of the copernicus trajectory design and optimization system," 4th International Conference on Astrodynamics Tools and Techniques, No. JSC-CN-20553, 2010.

[18] Gill, P.E., W. Murray and M.A. Saunders, "SNOPT: An SQP algorithm for large-scale constrained optimization", SIAM Review 47 (2005), 99-131.

[19] McCarty, S.L., "Parallel Monotonic Basin Hopping for Low Thrust Trajectory Optimization," 2018 Space Flight Mechanics Meeting, 2018, Orlando, Florida, January 2018.

[20] Biscani, F. and D. Izzo, "A parallel global multiobjective framework for optimization: pagmo", Journal of Open Source Software, vol. 5, #53, p. 2338, 2020.